RESEARCH ARTICLE

Dictionary Learning Method Based on K-Sparse Approximation and Orthogonal Procrustes Analysis for Reconstruction in Bioluminescence Tomography

Linzhi Su[1] | Limin Chen[1] | Wenlong Tang[1] | Huimin Gao[1] | Yi Chen[2] | Chengyi Gao[3] | Huangjian Yi[1] | Xin Cao[1]

[1]School of Information Science and Technology, Northwest University, Xi'an, China | [2]School of Electrical and Mechanical Engineering, The University of Adelaide, Adelaide, Australia | [3]Department of Oncology, The First Affiliated Hospital, Xi'an Jiaotong University, Xi'an, China

Correspondence: Yi Chen (yichen.cgz@gmail.com) | Xin Cao (caoxin918@hotmail.com)

ABSTRACT

Bioluminescence tomography (BLT) is one kind of noninvasive optical molecular imaging technology, widely used to study molecular activities and disease progression inside live animals. By combining the optical propagation model and inversion algorithm, BLT enables three-dimensional imaging and quantitative analysis of light sources within organisms. However, challenges like light scattering and absorption in tissues, and the complexity of biological structures, significantly impact the accuracy of BLT reconstructions. Here, we propose a dictionary learning method based on K-sparse approximation and Orthogonal Procrustes analysis (KSAOPA). KSAOPA uses an iterative alternating optimization strategy, enhancing solution sparsity with k-coefficients Lipschitzian mappings for sparsity(K-LIMAPS) in the sparse coding stage, and reducing errors with Orthogonal Procrustes analysis in the dictionary update stage, leading to stable and precise reconstructions. We assessed the method performance through simulations and in vivo experiments, which showed that KSAOPA excels in localization accuracy, morphological recovery, and in vivo applicability compared to other methods.

1 | Introduction

Bioluminescence imaging (BLI), as a highly sensitive noninvasive optical molecular imaging technique, has played a significant role in preclinical biomedical research for many years [1–3]. However, BLI mainly provides two-dimensional image information and cannot accurately locate the spatial position of the light source [1]. With the continuous deepening of biomedical research, the demand for 3D imaging of dynamic processes in vivo is becoming more and more intense, which promotes the development of BLT technology [2]. BLT is a powerful optical molecular three-dimensional imaging technology, which can reconstruct the three-dimensional distribution information of

the light source inside the organism from the light flux measured on the biological surface, using a light propagation model and computer inversion algorithms [4–6]. In recent years, BLT has been widely applied in cancer research, drug development, and efficacy evaluation due to its powerful three-dimensional imaging capabilities [7, 8]. Compared to BLI, BLT can more accurately locate and quantify biological light sources through 3D reconstruction, providing more detailed and intuitive three-dimensional imaging information, which offers important technical support for the field of biomedical research [9, 10].

However, the process of BLT reconstruction is significantly affected by factors such as the scattering and absorption effects

of light by biological tissues, as well as limitations in detecting photons at boundaries, leading to significant ill-posedness, and instability [11, 12]. These issues affect the accuracy and stability of reconstruction, with the result that suboptimal performance is observed in localization accuracy and target morphology recovery, thereby posing greater demands and challenges for reconstruction methods [11–13]. Therefore, there is a need for methods that can mitigate ill-posedness and effectively enhance reconstruction accuracy to satisfy various research requirements [14].

To alleviate the ill-posedness of BLT reconstruction and achieve more accurate reconstruction results, various solutions have been designed by researchers and scholars in recent years. For example, by optimizing the forward model, Chen et al. proposed a light propagation model based on a hybrid simplified spherical harmonics (SP_N) and diffusion equation (DE) [15]. This hybrid model can improve the modeling accuracy of photon transmission in biological tissues, thereby improving imaging quality. However, both the SP_N and the DE are approximation models of the radiative transfer equation (RTE), and transport errors due to the RTE approximation in various models are still inevitable. Based on deep-learning strategies, Rezaeifar et al. developed a novel deep-learning approach for tumor targeting and therapeutic planning in BLT studies [16]. The combination of flexibility, accuracy, and speed of deep learning solutions makes it a viable option for the BLT reconstruction problem, but the availability and quality of the training database remain a significant challenge. Combining prior information and norms, Wu et al. proposed an iterative reweighted L_2 norm optimization method that incorporates anatomical structure to enhance the performance of BLT [17]. In addition to anatomical structures, factors such as light source sparsity, multispectral information [18–21], light source feasible region [22–25], and optical characteristic parameters of biological tissues [26] are all important prior information for light source reconstruction. Among them, light source sparsity is one of the most commonly used prior information. Combined with this important prior information, many reconstruction methods based on sparse regularization have been proposed and widely applied in related research [27–29]. For instance, Leng et al. proposed a linearized Bregman iterative algorithm based on L_1 sparse regularization, which can accurately locate the position of the light source [30]. Yu et al. proposed a reconstruction algorithm based on $L_{1/2}$ regularization to enhance the sparsity of BLT reconstruction results [31]. However, these single regularization methods all have certain flaws. For example, L_1 norm regularization tends to result in over-sparsity issues [32, 33], while L_2 norm regularization can easily lead to over-smoothing [34]. Therefore, some joint regularization methods have been proposed by researchers to overcome these flaws [35, 36]. The biggest issue with current regularization methods is the selection of the optimal regularization parameter.

In this paper, a dictionary learning method based on K-sparse approximation and Orthogonal Procrustes analysis (KSAOPA) for BLT reconstruction is proposed to enhance the reconstruction accuracy. Compared to regularization methods, our approach effectively reduces the candidate set for the optimal parameters. Specifically, our method adopts an alternating optimization strategy as a whole, which includes two alternating parts: sparse coding and dictionary updating. In the sparse coding phase, compared with the orthogonal matching pursuit (OMP) algorithm [37] in traditional dictionary learning methods, K-sparse approximation not only ensures the sparsity of the bioluminescent source in space but also can obtain a more accurate approximation solution. In the dictionary updating phase, compared with the K-Singular value decomposition (K-SVD) algorithm [38] in traditional dictionary learning methods, Orthogonal Procrustes analysis can capture more complex data structures, improve efficiency, and reduce errors. To verify the reconstruction performance of our method, a series of numerical simulations and in vivo experiments were conducted, and comparisons were made with the incomplete variable truncation conjugate gradient method based on L_1 norm (IVTCG) [39], the morphological recovery method based on Gaussian weighted Laplacian prior regularization (GWLP) [40], and the k-coefficients Lipschitzian mappings for sparsity (K-LIMAPS) method [41].

The rest of this paper is structured as follows: In Section 2, the BLT forward model, the inverse problem of BLT reconstruction, and the proposed KSAOPA method are introduced. In Section 3, specific numerical simulation experiments and in vivo experiments are conducted to validate the performance of the reconstruction method. In Section 4, the corresponding experimental results are presented. Finally, in Section 5, the main work of this paper is discussed and concluded.

2 | Methodology

2.1 | The Photon Propagation Model and Inverse Problem of BLT

In BLT research, numerical model-based methods for BLT reconstruction typically employ a low-order approximate model of the RTE, such as the DE, to describe the process of photon transport within biological tissues. In the continuous wave mode, the steady-state domain DE combined with Robin boundary conditions is formulated as follows [42]:

$$\begin{cases} -\nabla[D(r)\nabla\Phi(r)] + \mu_a(r)\Phi(r) = S(r) & (r \in \Omega) \\ \Phi(r) + 2A(r)D(r)[v(r)\nabla\Phi(r)] = 0 & (r \in \partial\Omega) \end{cases} \quad (1)$$

where r is a point in the biological tissue region Ω, $\partial\Omega$ is the boundary of Ω, $\Phi(r)$ represents the photon flux rate at the point r, $S(r)$ is the energy density of the internal light source within the biological body, $A(r)$ stands for the boundary mismatch factor, $v(r)$ is the outward unit normal vector at the boundary $\partial\Omega$, and $D(r)$ is the diffusion coefficient at point r, which is calculated as follows:

$$D(r) = \frac{1}{3(\mu_a(r) + \mu_s'(r))} \quad (2)$$

where $\mu_a(r)$ and $\mu_s'(r)$ represent the absorption coefficient and reduced scattering coefficient, respectively.

Using the finite element method (FEM) to solve the aforementioned photon transport model, one can derive the mathematical

relationship between the photon flux Φ at the surface of the biological body and the internal unknown light source x as follows [43]:

$$\Phi = Ax \tag{3}$$

where A is an $m \times n$ dimensional system matrix; x is an n dimensional column vector representing the distribution of the light source within the biological body; and Φ represents the measured photon flux density on the surface of the biological body, which is an $m \times 1$ dimensional column vector.

2.2 | BLT Reconstruction Based on the KSAOPA Method

In the BLT reconstruction problem, due to the effects of light scattering and absorption, as well as the sparsity characteristic of the light source distribution, BLT reconstruction is a highly ill-posed problem, where the system matrix A is an ill-conditioned underdetermined matrix; hence, it is impossible to solve for x directly through Equation (3). To obtain a unique and stable numerical solution, based on knowledge of numerical analysis and related fields, we introduce L_p regularization to constrain and optimize Equation (3) [44], resulting in the following equation:

$$L = \|Ax - \Phi\|^2 + \lambda \|x\|_p \tag{4}$$

where λ is the regularization parameter, $\|x\|_p = \left(\sum_{i=1}^{n} |x_i|^p \right)^{1/p}$ represents the p-norm of vector x, and $\lambda \|x\|_p$ is the regularization term, known as the L_p norm, which serves as a penalty term to impose corresponding constraints on the objective function to obtain stable solutions.

Compared to the imaging object, the biological light source is sparse. Based on this prior knowledge, consider introducing sparse representation theory that is highly compatible with the BLT reconstruction problem. Sparse representation refers to representing a signal with as few atoms as possible in a given overcomplete dictionary, that is, expressing a known signal as a linear combination of a few atoms in the overcomplete dictionary, as shown in the following formula [45]:

$$y = w_1 \alpha_1 + w_2 \alpha_2 + \cdots + w_n \alpha_n = W\alpha \tag{5}$$

where $y \in \mathbb{R}^d$ represents a known signal sample, $W = [w_1, w_2, \cdots, w_n] \in \mathbb{R}^{d \times n}$ is an overcomplete dictionary, meaning $d < n$, and $\alpha = [\alpha_1, \alpha_2, \cdots, \alpha_n]^T$ is an n dimensional sparse coefficient vector. Equation (5) is an underdetermined equation, with infinitely many solutions for the coefficient vector α. To obtain a unique optimal solution, a regularizer is introduced. Based on the different types of norms used in the regularizer, sparse representation methods can be roughly divided into four categories: sparse representation based on L_0 norm minimization, sparse representation based on $L_p(0 < p < 1)$ norm minimization, sparse representation based on L_1 norm minimization, and sparse representation based on L_2 norm minimization. The objective functions of these four sparse representation methods are as follows [45]:

$$\begin{cases} \hat{\alpha} = \underset{\alpha}{argmin} \|\alpha\|_0 & s.t. \quad \|y - W\alpha\|_2^2 \leq \varepsilon \\ \hat{\alpha} = \underset{\alpha}{argmin} \|\alpha\|_p^p & s.t. \quad \|y - W\alpha\|_2^2 \leq \varepsilon \\ \hat{\alpha} = \underset{\alpha}{argmin} \|\alpha\|_1 & s.t. \quad \|y - W\alpha\|_2^2 \leq \varepsilon \\ \hat{\alpha} = \underset{\alpha}{argmin} \|\alpha\|_2^2 & s.t. \quad \|y - W\alpha\|_2^2 \leq \varepsilon \end{cases} \tag{6}$$

where ε is a small positive constant. Based on the sparse representation theory and regularization knowledge, considering the sparsity of light sources, in this study, we adopt the sparse representation based on L_0 norm minimization. Therefore, the objective function of the BLT reconstruction problem can be formulated as:

$$\underset{x}{argmin} \|\Phi - Ax\|_2^2 \quad s.t. \quad \|x\|_0 \leq K \tag{7}$$

where K represents the sparsity level of the vector x.

Based on sparse representation theory, the system matrix A in BLT reconstruction can be viewed as an overcomplete dictionary, with the vector x representing its corresponding sparse coefficients. The KSAOPA method considers the sparsity of light sources and adopts an alternating optimization scheme, which involves iteratively performing two steps: sparse coding and dictionary updating. The sparse coding part employs the K-LIMAPS algorithm [41], which exhibits good performance in sparse recovery and considers sparsity constraints on the reconstruction results. The dictionary updating part utilizes Orthogonal Procrustes analysis and singular value decomposition to optimize the system matrix [46], in order to reduce reconstruction errors.

2.2.1 | Sparse Coding

In the sparse coding part, the dictionary matrix A needs to be fixed to solve for the sparse coefficient vector x. Considering the sparsity of the reconstruction result, here, we use the K-LIMAPS algorithm to obtain an approximate solution for x. The K-LIMAPS algorithm is a fixed-point iterative method based on a nonlinear mapping that can uniformly enhance the sparsity at each iteration. During each iteration, each coefficient (vector element) either contracts (moves toward 0) or is retained (moves away from 0). It considers the sparsity constraint imposed on the objective function, which can limit the upper bound of the sparsity of the reconstruction result. This method is based on a nonlinear mapping operator, as described by the following formula:

$$f_\lambda(x) = x \odot \left(1 - e^{-\lambda|x|} \right) \tag{8}$$

where f_λ belongs to the parameter family of nonlinear functions $\mathcal{F} = \{f_\lambda \colon \mathbb{R}^m \to \mathbb{R}^m | \lambda \in \mathbb{R}^+\}$, $\odot$ denotes the Hadamard (element-wise) product, and λ is a positive real number.

The parameter λ is defined as follows: given a sparsity level K, let $\lambda_t = 1/\sigma_t$, where $\sigma_t = \hat{x}_{K+1}^{(t)}$, t represents the iteration

number, and $\hat{x}^{(t)}$ is obtained by rearranging the absolute values of $x^{(t)}$ in descending order, with $\hat{x}^{(t)}_{K+1}$ being the Kth element among them. Based on this strategy and the nonlinear operator, each coefficient x_i is multiplied by the penalty monotone function $g_\lambda(|x_i|) = 1 - e^{-\lambda|x_i|}$, which takes the specific form as follows:

$$\lim_{\lambda_t \to +\infty} g_{\sigma_t}\left(\left|x_i^{(t)}\right|\right) = 1 - e^{-\left|x_i^{(t)}\right|/\sigma_t} = \begin{cases} 1, & if\ i \in \Lambda^{(t)} \\ 0, & if\ i \in \Lambda_c^{(t)} \end{cases} \quad (9)$$

where the sets $\Lambda^{(t)}$ and $\Lambda_c^{(t)}$ are defined as follows:

$$\begin{cases} \Lambda^{(t)} = \left\{ i: \left|x_i^{(t)}\right| \le \sigma_t \right\} \\ \Lambda_c^{(t)} = \left\{ i: \left|x_i^{(t)}\right| > \sigma_t \right\} \end{cases} \quad (10)$$

Obviously, as $\lambda_t \to +\infty$, the following result can be obtained:

$$\lim_{\lambda_t \to +\infty} f_{\sigma_t}\left(x_i^{(t)}\right) = x_i^{(t)} g_{\sigma_t}\left(\left|x_i^{(t)}\right|\right) = \begin{cases} x_i^{(t)}, & if\ i \in \Lambda^{(t)} \\ 0, & if\ i \in \Lambda_c^{(t)} \end{cases} \quad (11)$$

Combining the nonlinear mapping operator and the orthogonal projection onto the null space of the dictionary matrix A, the update for the sparse coefficient vector x is as follows:

$$x^{(t+1)} = x^{(t)} - P\left[x^{(t)} \odot e^{-|x^{(t)}|/\sigma_t}\right] \quad (12)$$

where $P = I - Q$, with I being the identity matrix and $Q = A^+A$ representing the orthogonal projection onto the null space of the dictionary matrix A. Here, A^+ denotes the Moore-Penrose pseudoinverse of A, calculated as follows:

$$A^+ = \left(A^T A\right)^{-1} A^T \quad (13)$$

Algorithm 1 summarizes the process of the K-LIMAPS algorithm.

ALGORITHM 1 | K-LIMAPS.

Input: a dictionary matrix A, its pseudo-inverse A^+, a signal Φ, sparsity level K.

Initialization: $t_{\max} = 10$, current iteration $t = 1$.

1. $x \leftarrow A^+\Phi$

2. $P \leftarrow I - A^+A$

3. **While** $t \le t_{\max}$ do

4. $\quad \sigma \leftarrow sort(|x|)$

5. $\quad \lambda \leftarrow 1/\sigma_t$

6. $\quad x \leftarrow x - P\left[x \odot e^{-\lambda|x|}\right]$

7. **End while**

8. $x_i \leftarrow 0\ \ \forall i\ s.t.\ |x|_0 \le K$

Output: x

2.2.2 | Dictionary Update

In the dictionary update part, with the sparse coefficient vector x fixed, the objective function for solving the dictionary matrix A is as follows:

$$\underset{A}{argmin} \|\Phi - Ax\|_2^2 \quad s.t. \quad \|x\|_0 \le K \quad (14)$$

To reduce reconstruction error, we use Orthogonal Procrustes analysis and singular value decomposition to optimize the dictionary matrix A in the dictionary update. Procrustes analysis is a method for comparing the consistency of two sets of data by analyzing shape distributions. Mathematically, it is implemented through iterative processes to find a standard shape and use the least squares method to find the affine transformation (such as translation, rotation, and scaling) of each object shape to this standard shape. When the allowed transformations are limited to orthogonal transformations, it is called Orthogonal Procrustes analysis.

The algorithmic idea for the dictionary update stage using Orthogonal Procrustes analysis and singular value decomposition is as follows:

1. At each iteration, partition the column index set $[n] = \{1, 2, \cdots, n\}$ of the dictionary matrix A into G subsets of equal size, denoted as $[n] = I_1 \bigcup I_2 \bigcup \cdots \bigcup I_G$, where each subset contains s elements (indices), i.e., $s = |I_g|$, $g \in \{1, 2, \cdots, G\}$, $G = \lceil n/s \rceil$. If n is not a multiple of s, then $|I_G| = n - (G-1)s$, where s is manually adjusted.

2. Corresponding to each column index subset $I_1, I_2, \cdots, I_G$, partition the dictionary matrix A into G subdictionaries $A_{I_1}, A_{I_2}, \cdots, A_{I_G}$. Then decompose the product Ax into the following form:

$$Ax = A_I x_I + A_{I^c} x_{I^c} \quad (15)$$

where A_I represents a subdictionary of $m \times s$ dimensions formed by the columns of A indexed by the set I, i.e., $I \in \{I_1, I_2, \cdots, I_G\}$ and $A_I \in \{A_{I_1}, A_{I_2}, \cdots, A_{I_G}\}$. x_I is the subvector formed by the rows of x indexed by the set I, with dimensions $s \times 1$. A_{I^c} is the complement of the subdictionary A_I in the dictionary A, and x_{I^c} is the complement of the subvector x_I in the vector x. Thus, the objective function can be written as:

$$\underset{A}{argmin} \|\Phi - Ax\|_2^2 = \left\|\Phi - A_{I^c} x_{I^c} - A_I x_I\right\|_2^2 \quad s.t. \quad \|x\|_0 \le K \quad (16)$$

Therefore, the update problem for the entire dictionary matrix A is transformed into the update problem for each subdictionary A_I after grouping.

3. Using Orthogonal Procrustes analysis and singular value decomposition to update each subdictionary A_I, thereby obtaining the updated values A' for the entire dictionary matrix A. For each subdictionary A_I, introducing an m-dimensional orthogonal transformation matrix R to solve for the updated value A'_I, the computation can be calculated as follows:

$$A'_I = RA_I \quad (17)$$

For this, the following minimization problem can be obtained:

$$\underset{R}{argmin}\|E - RH\|_2^2 \qquad (18)$$

This problem is known as the Orthogonal Procrustes problem, where $E = \Phi - A_{I^c}x_{I^c}$ and $H = A_I x_I \in \mathbb{R}^{m \times 1}$, which can be interpreted as finding the rotation of the subspace matrix H^T to closely approximate the subspace matrix E^T.

The Orthogonal Procrustes problem has an optimal solution $\hat{R}$, which can be calculated based on the orthogonal matrices U and V obtained from the singular value decomposition $EH^T = U\Sigma V^T \in \mathbb{R}^{m \times m}$, where Σ is a diagonal matrix with the singular values of EH^T on its diagonal. The computation of $\hat{R}$ is given by the following formula:

$$\hat{R} = VU^T \qquad (19)$$

By substituting the result $\hat{R}$ from Equation (19) into Equation (17), we can obtain the updated value $A_I{}'$ for each subdictionary A_I. Upon completion of the updates for all subdictionaries, the update of the entire dictionary matrix A is also completed.

In summary, the process of the KSAOPA method is summarized as shown in Algorithm 2.

3 | Experiment Design

To validate and evaluate the effectiveness of the KSAOPA method proposed in Section 2 for the BLT reconstruction problem, we designed several numerical simulation experiments and an in vivo mouse experiment. We compared our method with three other algorithms: IVTCG, GWLP, and K-LIMAPS, in terms of localization accuracy, morphological recovery,

---

ALGORITHM 2 | KSAOPA for BLT Reconstruction.

Input: The system matrix $A \in \mathbb{R}^{m \times n}$, the detected surface photon $\Phi \in \mathbb{R}^{m \times 1}$, sparsity level K.
Initialization: $x^0 = 0, err = 1e - 6, k_{max} = 10$, current iteration $k = 1$, index subcollection size s, the number of subdictionaries $G = \lceil n/s \rceil$.
While $\|x^k - x^{k-1}\|_2 > err$ or $k < k_{max}$ **do**
  step1: Sparse coding using Algorithm 1
  Partition indices $[n] = I_1 \bigcup I_2 \bigcup \cdots \bigcup I_G$
  step2: Dictionary update
  for $g = 1, 2, \cdots, G$ **do**
    $I = I_g$
    $E = \Phi - A_{I^c}x_{I^c}$
    $H = A_I x_I$
    $EH^T = U\Sigma V^T$
    $R = \underset{R}{argmin}\|E - RH\|_2^2 = VU^T$
    $A_I = R\hat{A}_I$
  end for
  step3: $k = k + 1$
End while
Output: $x = x^k$

---

robustness, and in vivo applicability. All experiments and procedures were conducted on a laptop equipped with an Intel(R) Core (TM) i5-9300H CPU (2.40 GHz) and 8 GB RAM.

3.1 | Numerical Simulations

In the numerical simulation experiments, we used a heterogeneous cylindrical model with a height of 30 mm and a radius of 10 mm, as shown in the 3D view in Figure 1a. This model comprises five organs: muscle, bone, heart, lung, and liver. The optical parameters of these organs at a wavelength of 650 nm are listed in Table 1. For the BLT reconstruction, the model was discretized into a tetrahedral mesh containing 4626 nodes and 25 840 tetrahedral elements using COMSOL Multiphysics software [47], as illustrated in Figure 1b. Figure 1c shows the forward simulation results of a spherical light source with a radius of 1 mm, generated using the molecular optical simulation environment (MOSE) [48] based on the Monte Carlo method.

Three sets of experiments were conducted in the cylindrical model: single light source simulation experiment, dual light source simulation experiment, and antinoise experiment. In the single light source experiment, a spherical light source with a radius of 1 mm and a center point at $(-5, -6, 12)$ was set to simulate an actual bioluminescent source. In the dual light source experiment, two spherical light sources with radii of 1 mm and center points at $(-7, 5, 5)$ and $(-7, 5, 12)$ were set to simulate two actual bioluminescent sources. These two simulation experiments were designed to evaluate the performance of the KSAOPA method in terms of localization accuracy and morphology recovery. In the antinoise experiment, Gaussian noise levels of 5%, 10%, 15%, 20%, and 25% were added to the single light source experiment to assess the robustness of the KSAOPA method based on the results of the noise resistance experiments.

3.2 | In Vivo Experiment

To assess the practicality of the KSAOPA method in live animal research, we conducted in vivo experiments on live mice. All experimental procedures were approved by the Animal Ethics Committee of Northwest University in China. We used an adult BALB/c mouse for the in vivo experiment and administered a 3% isoflurane-air mixture anesthesia to the mouse during surgery to alleviate its pain.

During the experimental process, we imaged an adult nude mouse using a BLT/CT dual-modality tomographic scanning system. First, we implanted a luminescent tube with a radius of 1 mm and a height of 2 mm as a biological light source within the mouse, containing 10 μL of luminescent solution. The luminescent tube was made of plastic material to facilitate precise positioning of the actual light source area when detected using CT. Then, we fixed the anesthetized mouse on a rotating platform and kept it still during the imaging process. To capture the bioluminescence images, we used an EMCCD camera (Ixon Ultra 888) to photograph the surface luminescence images, employing a 630 nm band-pass filter to enhance the imaging quality. When the EMCCD camera

FIGURE 1 | (a) The 3D view of the cylindrical model. (b) The 3D view of the tetrahedral mesh. (c) The forward simulation result of the single light source.

TABLE 1 | The optical parameters in numerical simulation.

Tissues	$\mu_a\,(\mathrm{mm}^{-1})$	$\mu_s\,(\mathrm{mm}^{-1})$	g
Muscle	0.0052	10.80	0.900
Heart	0.0083	6.733	0.850
Liver	0.0329	7.000	0.900
Lung	0.0133	19.70	0.900
Bone	0.0060	60.09	0.900

was operating, the exposure time was set to 1 s without any gain value. To obtain the CT images, we imaged the mouse using the CT system (tube voltage 50 kVp, x-ray power 40 W) within the dual-modality imaging device. Figure 2 shows a schematic diagram of the BLT/CT dual-modality imaging system structure.

Next, we processed the collected data. A landmark-based rigid registration method was used to register the CT data with the bioluminescence images. After registration, the absolute irradiance distribution in the two-dimensional optical images was projected onto the three-dimensional surface of the mouse model. Amira software was utilized to segment the main organs of the mouse, including muscles, heart, lungs, liver, stomach, and kidneys, and the mouse model was discretized into a tetrahedral mesh containing 4118 nodes and 22970 tetrahedral elements for BLT reconstruction. The coordinates of the implanted real light source were (19.6, 13.5, 22.3) mm. To evaluate the in vivo practicality of the KSAOPA method, we compared it with the other three algorithms previously mentioned. Figure 3 illustrates the 3D view of the mouse model and its tetrahedral mesh.

3.3 | Evaluation Metrics

To analyze and evaluate the performance of BLT reconstruction results in terms of localization accuracy and shape

recovery, this study employed two commonly used evaluation metrics, namely the localization error (LE) and the Dice coefficient (DICE) [49].

LE represents the Euclidean distance between the reconstructed light source center (x_r, y_r, z_r) and the actual light source center (x_0, y_0, z_0). It is used to measure the localization accuracy of the reconstruction results. A smaller LE value indicates higher localization accuracy. The calculation is as follows:

$$LE = \sqrt{(x_r - x_0)^2 + (y_r - y_0)^2 + (z_r - z_0)^2} \tag{20}$$

To evaluate the morphological recovery ability of the algorithm, the DICE is used as an evaluation metric, which indicates the degree of overlap between the reconstructed light source region X_r and the actual light source region Y. The DICE value ranges from 0 to 1, and the closer it is to 1, the higher the overlap between the reconstructed and actual light source regions, indicating better shape recovery performance of the algorithm.

$$Dice = \frac{2|X_r \bigcap Y|}{|X_r| + |Y|} \tag{21}$$

4 | Results

## 4.1 | Numerical Simulations Results

4.1.1 | Single Light Source Experiment

The reconstruction results of the single light source simulation experiment are shown in Figure 4. The first row displays the 3D views of the reconstruction results for the IVTCG, GWLP, K-LIMAPS, and KSAOPA methods, where the red areas indicate the reconstructed light sources. The second row shows the axial views corresponding to the reconstruction outcomes of the different methods, with the cyan areas denoting the reconstructed light sources and the black circles signifying the positions of the
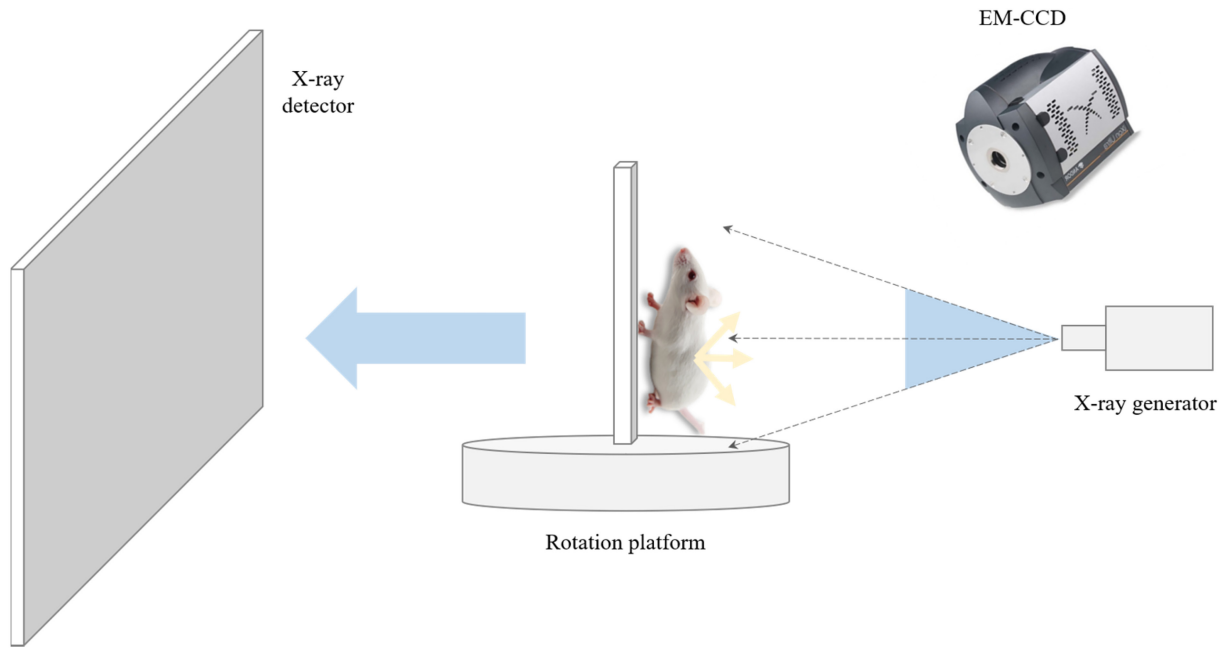
**FIGURE 2** | Schematic diagram of the BLT/CT imaging system.
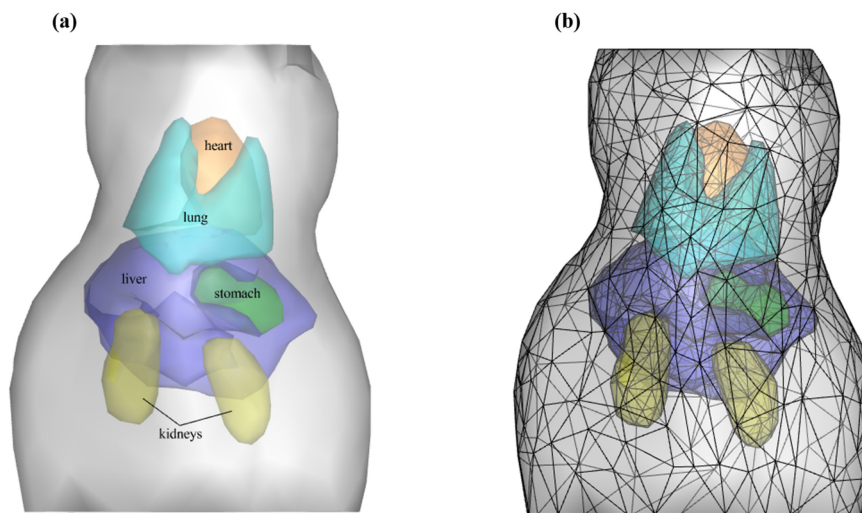
FIGURE 3 | (a) In vivo mouse model. (b) The 3D view of the tetrahedral mesh.

actual light sources. It is observable from the images that the light source reconstructed by our method has the highest spatial overlap with the true light source. The quantitative assessment of the four reconstruction methods is detailed in Table 2. Apparently, when compared to the other three methods, the KSAOPA method has the lowest LE and the highest DICE, demonstrating that the reconstruction results of KSAOPA more closely approximate the actual light source in terms of localization accuracy and shape recovery, outperforming the other three algorithms.

4.1.2 | Dual Light Source Experiment

The reconstruction results of the dual light source simulation experiment are shown in Figure 5. The first row displays the 3D views of the reconstruction results for the four methods, and the second row shows the axial views of the reconstruction results for the four methods. The representation of the reconstructed and actual light sources is consistent with that in the single light source experiment. From Figure 5, it can be seen that compared with the other three methods, the KSAOPA method has better localization accuracy and spatial overlap, and its reconstruction performance is superior to the other three methods. Table 3 presents the quantitative analysis results of the four reconstruction methods, confirming this point. The results show that compared to the other three methods, the individual LE values of the KSAOPA method are the lowest and more uniform, with the lowest average LE value. At the same time, the individual DICE values of the KSAOPA method are all higher than the results of the GWLP and K-LIMAPS methods. Compared with the IVTCG method,
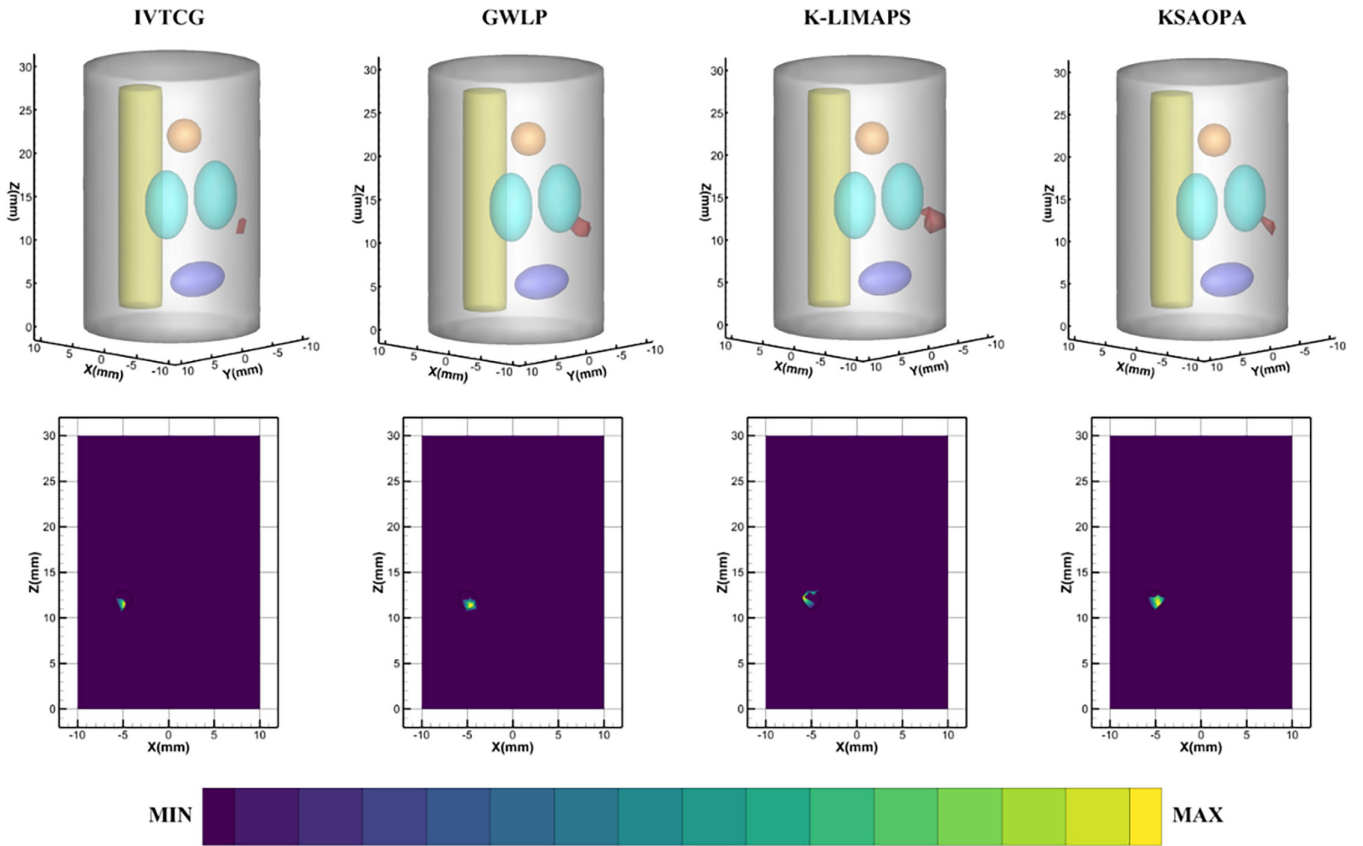
FIGURE 4 | Reconstruction results of the single light source experiment for four methods.

TABLE 2 | Quantitative results of different methods in the single light source experiment.

Method	Real region center (mm)	Reconstructed region center (mm)	LE (mm)	DICE
IVTCG	(−5.00, −6.00, 12.00)	(−4.669, −5.874, 11.359)	0.732	0.358
GWLP	(−5.00, −6.00, 12.00)	(−4.624, −5.826, 11.540)	0.620	0.416
K-LIMAPS	(−5.00, −6.00, 12.00)	(−5.332, −6.238, 12.108)	0.423	0.328
KSAOPA	(−5.00, −6.00, 12.00)	(−4.780, −6.143, 11.829)	0.313	0.758

although the DICE value at the point (−7, 5, 5) is the same, both being 0.667, at the point (−7, 5, 12), the DICE value of the KSAOPA method is 0.634, higher than the 0.388 of the IVTCG method, and more uniform. Clearly, compared to the other three methods, the DICE value results of the KSAOPA method are better, and it has the lowest average DICE value. In summary, the KSAOPA method has better performance in terms of dual light source localization accuracy and morphological recovery.

4.1.3 | Antinoise Experiment

The results of the antinoise experiment are shown in Figure 6. To evaluate the robustness of the KSAOPA method, we added 5%, 10%, 15%, 20%, and 25% Gaussian noise to the measurement data based on the single light source experiment to test the impact of Gaussian noise on the reconstruction results. As can be seen from Figure 6, after adding different proportions

of Gaussian noise, the fluctuations in the LE values and DICE are relatively small, and the reconstruction performance of the KSAOPA method does not decline, indicating that our method has good robustness.

4.2 | In Vivo Experiment Results

The reconstructed results of in vivo experiments are shown in Figure 7. Figure 7 displays the 3D and axial views of the reconstruction results for four different methods, with the red area in the 3D view representing the reconstructed light source. Table 4 provides the quantitative analysis results for the four reconstruction methods. From the quantitative analysis results, it is evident that compared to the other three methods, the KSAOPA method has the smallest LE value and the largest DICE value, indicating that the KSAOPA method exhibits better performance in terms of localization accuracy and morphological restoration, while also demonstrating its excellent practicality for in vivo applications.
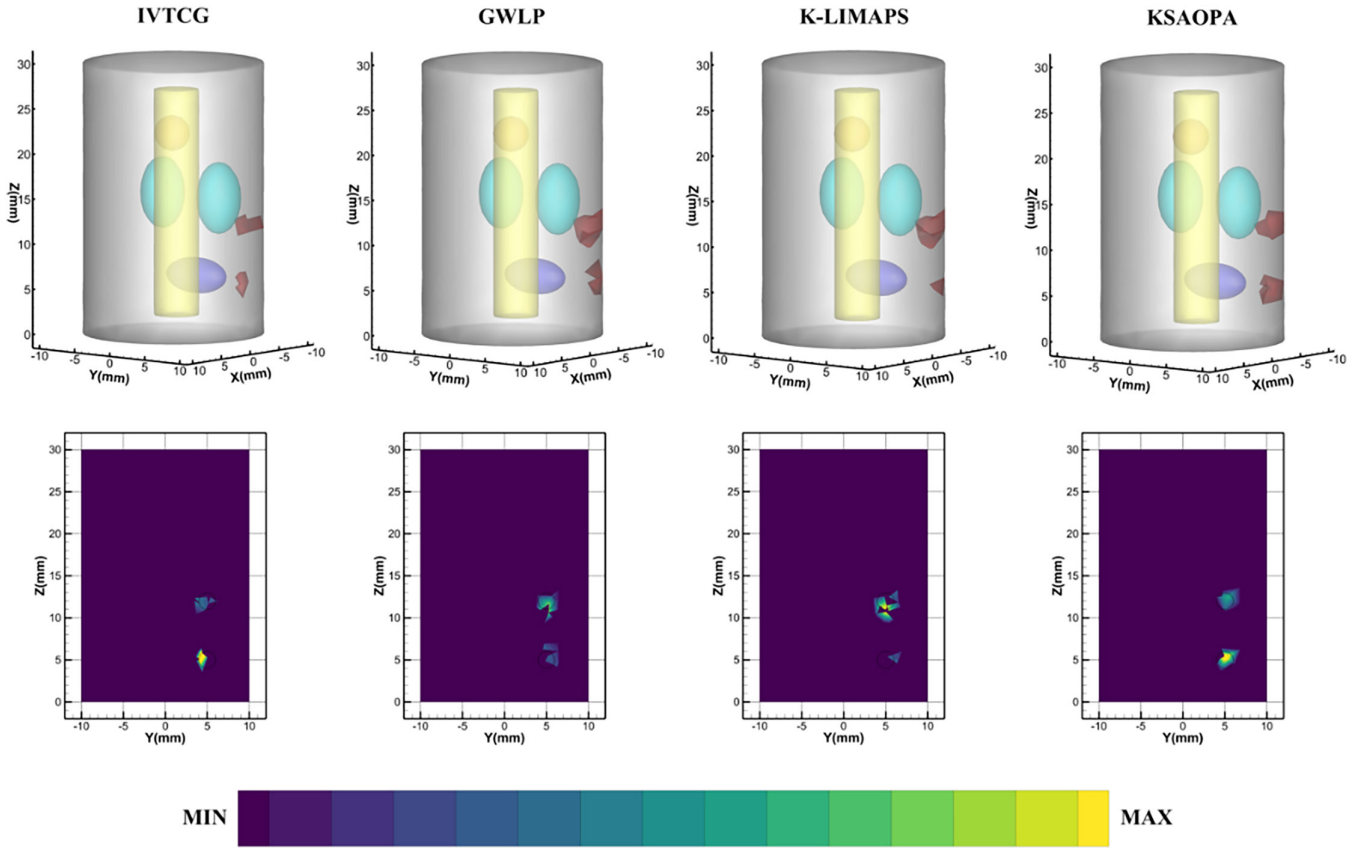
FIGURE 5 | Reconstruction results of the dual light source experiment for four methods.

TABLE 3 | Quantitative results of different methods in the dual light source experiment.

Method	Real region center (mm)	LE (mm)	AVG LE (mm)	DICE	AVG DICE
IVTCG	(−7.00, 5.00, 5.00)	0.941	0.995	0.667	0.527
	(−7.00, 5.00, 12.00)	1.050		0.388	
GWLP	(−7.00, 5.00, 5.00)	1.100	0.871	0.299	0.363
	(−7.00, 5.00, 12.00)	0.643		0.426	
K-LIMAPS	(−7.00, 5.00, 5.00)	0.989	0.877	0.330	0.343
	(−7.00, 5.00, 12.00)	0.765		0.356	
KSAOPA	(−7.00, 5.00, 5.00)	0.431	0.468	0.667	0.650
	(−7.00, 5.00, 12.00)	0.506		0.634	

5 | Discussion and Conclusions

BLT is a powerful noninvasive optical molecular imaging technique that offers advantages such as low cost and high sensitivity. However, the reconstruction problem in BLT is affected by factors such as the effects of light scattering and absorption, as well as the complexity of biological tissue structure, exhibiting serious ill-posedness and instability, which leads to poor imaging quality. In order to enhance the reconstruction accuracy of BLT and improve image quality, this paper proposes a method called KSAOPA for sparse reconstruction in BLT. This method is based on the prior knowledge that the light sources have sparsity, and aims to improve the reconstruction quality by alleviating the ill-posedness of the inverse problem. The KSAOPA method, grounded in sparse representation theory and

dictionary learning methods, employs an iterative alternating optimization strategy. The alternating part includes two steps: sparse coding and dictionary update. In the sparse coding part, the K-LIMAPS algorithm is utilized to ensure the sparsity of the solution, and in the dictionary update, Orthogonal Procrustes analysis is introduced to optimize the system matrix, reduce reconstruction errors, and thereby obtain more accurate reconstruction results.

To evaluate the performance of the proposed KSAOPA method, a series of numerical simulation experiments and in vivo experiments were designed, and comparisons were made with three other methods: IVTCG, GWLP, and K-LIMAPS. The results of the single and dual light source simulation experiments demonstrated the superior performance of the KSAOPA method in
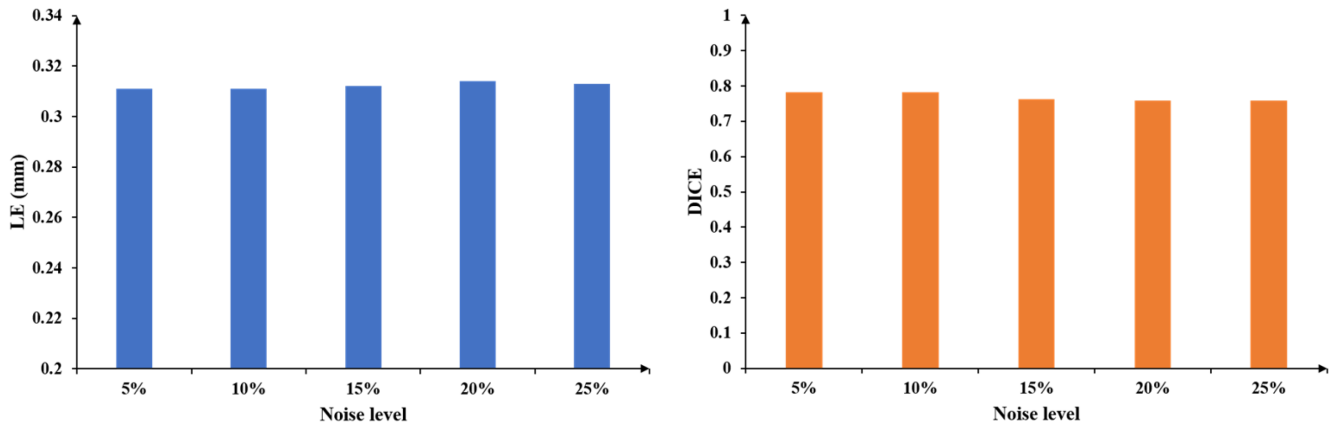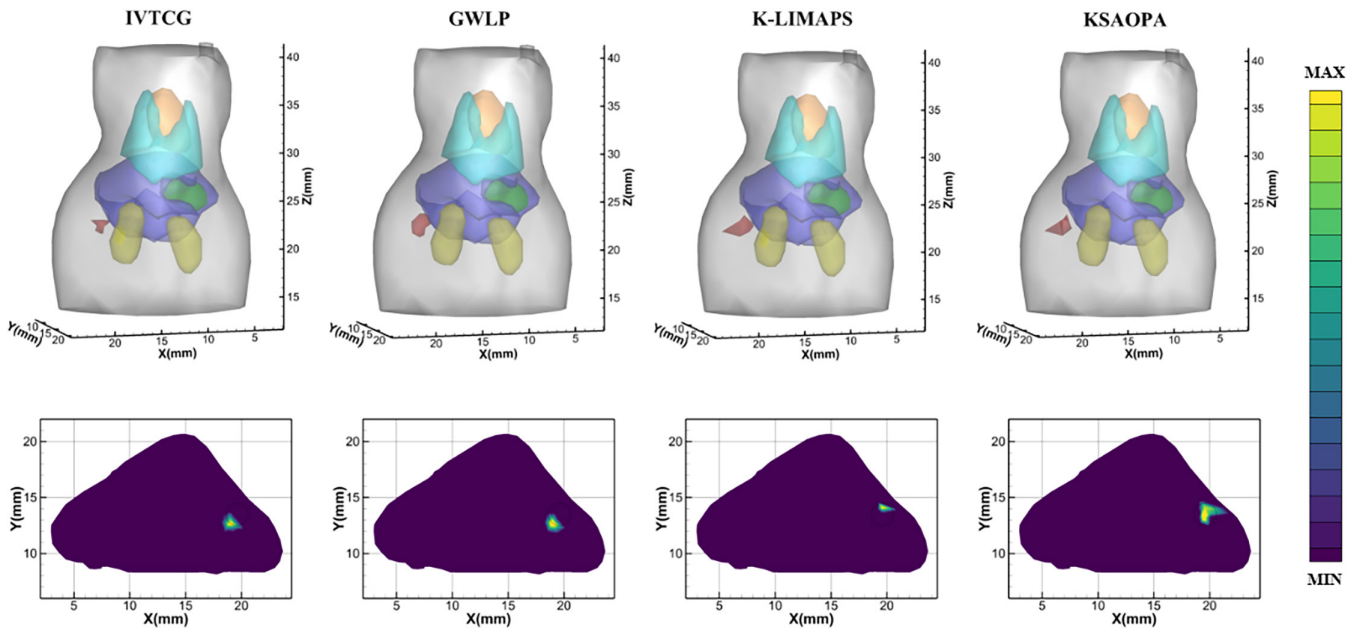
FIGURE 6 | Results of the antinoise experiment.

FIGURE 7 | Reconstruction results of the in vivo experiment.

TABLE 4 | Quantitative results of in vivo experiment.

Method	Real region center (mm)	Reconstructed region center (mm)	LE (mm)	DICE
IVTCG	(19.60, 13.50, 22.30)	(19.064, 12.596, 22.151)	1.062	0.256
GWLP	(19.60, 13.50, 22.30)	(19.201, 12.635, 22.184)	0.959	0.144
K-LIMAPS	(19.60, 13.50, 22.30)	(19.659, 14.005, 22.816)	0.725	0.165
KSAOPA	(19.60, 13.50, 22.30)	(19.635, 13.634, 22.638)	0.365	0.726

terms of localization accuracy and shape recovery. The antinoise experiment results showed that the KSAOPA method has good robustness against noise. The in vivo experimental results illustrated the feasibility and practicality of the KSAOPA method in medical research on live animals. Moreover, all experimental results indicated that the KSAOPA method outperforms the other three comparison methods, achieving more precise reconstruction outcomes.

However, although the KSAOPA method has demonstrated good performance in BLT reconstruction, it still has some limitations. First, some parameters used in the KSAOPA method require manual adjustment, such as the sparsity level K; it is necessary to propose an adaptive parameter selection algorithm to automatically adjust these parameters. Second, whether the KSAOPA method can be applied to other modalities of optical molecular tomography needs further verification to assess its universality.

Additionally, the potential of the KSAOPA method in clinical applications of BLT should be further evaluated. Therefore, in future work, we need to address these limitations and refine the KSAOPA method. For instance, the issue of manual parameter selection should be resolved, and the universality of the KSAOPA method should be verified. By addressing these limitations, the method can play a greater role in biomedical clinical research.

In summary, we proposed a dictionary learning method based on KSAOPA to enhance the accuracy of BLT reconstruction. By alternately performing sparse coding and dictionary update, the KSAOPA method not only alleviates the ill-posedness of the problem and ensures the sparsity of the solution, but also optimizes the system matrix and reduces reconstruction errors. We assessed the performance of this method by designing a series of numerical simulation experiments and in vivo experiments, comparing it with other reconstruction methods. The experimental results show that the KSAOPA method has superior performance in localization accuracy and shape recovery, and has good robustness and in vivo practicability in BLT reconstruction. This method improves reconstruction precision and can obtain more accurate and stable reconstruction results. We believe that our method will be beneficial to various biomedical clinical studies of BLT.

Conflicts of Interest

The authors declare no conflicts of interest.

Data Availability Statement

The data that support the findings of this study are available from the corresponding author upon reasonable request.

References

1. L. Yin, K. Wang, T. Tong, et al., "Adaptive Grouping Block Sparse Bayesian Learning Method for Accurate and Robust Reconstruction in Bioluminescence Tomography," *IEEE Transactions on Biomedical Engineering* 68 (2021): 3388–3398.

2. S. Ren, L. Wang, Q. Zeng, D. Chen, X. Chen, and J. Liang, "Effective Reconstruction of Bioluminescence Tomography Based on GPU-Accelerated Inverse Monte Carlo Method," *AIP Advances* 10 (2020): 105329.

3. G. Wang, Y. Li, and M. Jiang, "Uniqueness Theorems in Bioluminescence Tomography," *Medical Physics* 31 (2004): 2289–2299.

4. W. Cong, G. Wang, D. Kumar, et al., "Practical Reconstruction Method for Bioluminescence Tomography," *Optics Express* 13 (2005): 6756–6771.

5. A. Bentley, X. Xu, Z. Deng, J. E. Rowe, K. Kang-Hsin Wang, and H. Dehghani, "Quantitative Molecular Bioluminescence Tomography," *Journal of Biomedical Optics* 27 (2022): 066004.

6. H. Dehghani, S. C. Davis, and B. W. Pogue, "Spectrally Resolved Bioluminescence Tomography Using the Reciprocity Approach," *Medical Physics* 35 (2008): 4863–4871.

7. D. Yang, L. Wang, D. Chen, et al., "Filtered Maximum Likelihood Expectation Maximization Based Global Reconstruction for Bioluminescence Tomography," *Medical & Biological Engineering & Computing* 56 (2018): 2067–2081.

8. H. Guo, J. Yu, Z. Hu, H. Yi, Y. Hou, and X. He, "A Hybrid Clustering Algorithm for Multiple-Source Resolving in Bioluminescence Tomography," *Journal of Biophotonics* 11 (2018): e201700056.

9. S. Mollard, R. Fanciullino, S. Giacometti, C. Serdjebi, S. Benzekry, and J. Ciccolini, "In Vivo Bioluminescence Tomography for Monitoring Breast Tumor Growth and Metastatic Spreading: Comparative Study and Mathematical Modeling," *Scientific Reports* 6 (2016): 36173.

10. H. Hu, J. Liu, L. Yao, et al., "Real-Time Bioluminescence and Tomographic Imaging of Gastric Cancer in a Novel Orthotopic Mouse Model," *Oncology Reports* 27 (2012): 1937–1943.

11. Y. Lv, J. Tian, W. Cong, et al., "A Multilevel Adaptive Finite Element Algorithm for Bioluminescence Tomography," *Optics Express* 14 (2006): 8211–8223.

12. H. Guo, L. Gao, J. Yu, et al., "Sparse-Graph Manifold Learning Method for Bioluminescence Tomography," *Journal of Biophotonics* 13 (2020): e201960218.

13. Y. Liu, H. Guo, Y. Xiao, W. Li, and J. Yu, "Hybrid Reconstruction Framework for Model-Based Multispectral Bioluminescence Tomography Based on Alpha-Divergence," *Journal of Innovative Optical Health Sciences* 16 (2023): 2245003.

14. K. Wang, C. Chi, Z. Hu, et al., "Optical Molecular Imaging Frontiers in Oncology: The Pursuit of Accuracy and Sensitivity," *Engineering* 1 (2015): 309–323.

15. X. Chen, F. Sun, D. Yang, S. Ren, Q. Zhang, and J. Liang, "Hybrid Simplified Spherical Harmonics With Diffusion Equation for Light Propagation in Tissues," *Physics in Medicine & Biology* 60 (2015): 6305–6322.

16. B. Rezaeifar, C. J. A. Wolfs, N. G. Lieuwes, et al., "A Deep-Learning Assisted Bioluminescence Tomography Method to Enable Radiation Targeting in Rat Glioblastoma," *Physics in Medicine and Biology* 68 (2023): 155013.

17. P. Wu, Y. Hu, K. Wang, and J. Tian, "Bioluminescence Tomography by an Iterative Reweighted l2-Norm Optimization," *IEEE Transactions on Biomedical Engineering* 61 (2013): 189–196.

18. Z. Hu, C. Fang, B. Li, et al., "First-In-Human Liver-Tumour Surgery Guided by Multispectral Fluorescence Imaging in the Visible and Near-Infrared-I/II Windows," *Nature Biomedical Engineering* 4 (2020): 259–271.

19. J. Feng, K. Jia, G. Yan, et al., "An Optimal Permissible Source Region Strategy for Multispectral Bioluminescence Tomography," *Optics Express* 16 (2008): 15640–15654.

20. D. Chen, S. Zhu, X. Chen, et al., "Quantitative Cone Beam X-Ray Luminescence Tomography/X-Ray Computed Tomography Imaging," *Applied Physics Letters* 105 (2014): 191104.

21. K. Liu, X. Yang, D. Liu, et al., "Spectrally Resolved Three-Dimensional Bioluminescence Tomography With a Level-Set Strategy," *Journal of the Optical Society of America A* 27 (2010): 1413–1423.

22. C. Qin, S. Zhu, J. Feng, et al., "Comparison of Permissible Source Region and Multispectral Data Using Efficient Bioluminescence Tomography Method," *Journal of Biophotonics* 4 (2011): 824–839.

23. H. Huang, X. Qu, J. Liang, et al., "A Multi-Phase Level set Framework for Source Reconstruction in Bioluminescence Tomography," *Journal of Computational Physics* 229 (2010): 5246–5256.

24. H. Zhang, L. Hai, J. Kou, et al., "OPK_SNCA: Optimized Prior Knowledge via Sparse Non-convex Approach for Cone-Beam X-Ray Luminescence Computed Tomography Imaging," *Computer Methods and Programs in Biomedicine* 215 (2022): 106645.

25. C. Qin, J. Feng, S. Zhu, et al., "Recent Advances in Bioluminescence Tomography: Methodology and System as Well as Application," *Laser & Photonics Reviews* 8 (2014): 94–114.

26. Z. Hu, J. Liang, W. Yang, et al., "Experimental Cerenkov Luminescence Tomography of the Mouse Model With SPECT Imaging Validation," *Optics Express* 18 (2010): 24441–24450.

27. W. Guo, K. Jia, D. Han, et al., "Efficient Sparse Reconstruction Algorithm for Bioluminescence Tomography Based on Duality and Variable Splitting," *Applied Optics* 51 (2012): 5676–5685.

28. M. Yukawa and S. I. Amari, "Lp -Regularized Least Squares (0< p<1) and Critical Path," *IEEE Transactions on Information Theory* 62 (2015): 488–502.

29. J. Yu, F. Liu, J. Wu, L. Jiao, and X. He, "Fast Source Reconstruction for Bioluminescence Tomography Based on Sparse Regularization," *IEEE Transactions on Biomedical Engineering* 57 (2010): 2583–2586.

30. C. Leng, D. Yu, S. Zhang, Y. An, and Y. Hu, "Reconstruction Method for Optical Tomography Based on the Linearized Bregman Iteration With Sparse Regularization," *Computational and Mathematical Methods in Medicine* 2015 (2015): 304191.

31. J. Yu, Q. Li, and H. Wang, "Source Reconstruction for Bioluminescence Tomography via L 1/ 2 Regularization," *Journal of Innovative Optical Health Sciences* 11 (2018): 1750014.

32. C. Chen, F. Tian, H. Liu, and J. Huang, "Diffuse Optical Tomography Enhanced by Clustered Sparsity for Functional Brain Imaging," *IEEE Transactions on Medical Imaging* 33 (2014): 2323–2331.

33. T. Liu, J. Rong, P. Gao, et al., "Regularized Reconstruction Based on Joint L 1 and Total Variation for Sparse-View Cone-Beam x-Ray Luminescence Computed Tomography," *Biomedical Optics Express* 10 (2019): 1–17.

34. N. Cao, A. Nehorai, and M. Jacob, "Image Reconstruction for Diffuse Optical Tomography Using Sparsity Regularization and Expectation-Maximization Algorithm," *Optics Express* 15 (2007): 13695–13708.

35. M. Chu, H. Guo, X. He, et al., "A Graph-Guided Hybrid Regularization Method for Bioluminescence Tomography," *Computer Methods and Programs in Biomedicine* 230 (2023): 107329.

36. J. Feng, Y. Li, Z. Li, Z. Sun, and K. Jia, "A Reconstruction Algorithm for Bioluminescence Tomography Based on Sparse and Total Variation Regularizations," in *Microscopy Histopathology and Analytics* (Hollywood, FL: Optica Publishing Group, 2018), JTu3A.28.

37. L. Denis, D. A. Lorenz, and D. Trede, "Greedy Solution of Ill-Posed Problems: Error Bounds and Exact Inversion," *Inverse Problems* 25 (2009): 115017.

38. M. Aharon, M. Elad, and A. Bruckstein, "K-SVD: An Algorithm for Designing Overcomplete Dictionaries for Sparse Representation," *IEEE Transactions on Signal Processing* 54 (2006): 4311–4322.

39. X. He, J. Liang, X. Wang, et al., "Sparse Reconstruction for Quantitative Bioluminescence Tomography Based on the Incomplete Variables Truncated Conjugate Gradient Method," *Optics Express* 18 (2010): 24825–24841.

40. Y. Gao, K. Wang, S. Jiang, Y. Liu, T. Ai, and J. Tian, "Bioluminescence Tomography Based on Gaussian Weighted Laplace Prior Regularization for in Vivo Morphological Imaging of Glioma," *IEEE Transactions on Medical Imaging* 36 (2017): 2343–2354.

41. A. Adamo and G. Grossi, "A Fixed-Point Iterative Schema for Error Minimization in K-Sparse Decomposition," in *2011, IEEE International Symposium on Signal Processing and Information Technology (ISSPIT)* (Bilbao, Spain: IEEE, 2011), 167–172.

42. J. Huang and J. Yu, "Bioluminescence Tomography Based on Multilevel Adaptive Finite Element Method," *Chinese Journal of Lasers* 45 (2018): 607003.

43. H. Guo, H. Zhao, X. Song, and X. He, "Alternating Direction Method of Multipliers Network for Bioluminescence Tomography Reconstruction," in *IEEE Engineering in Medicine & Biology Society* (Mexico: IEEE, 2021), 3109–3113.

44. H. Zhang, G. Geng, S. Zhang, et al., "Sparse Non-Convex lp Regularization for Cone-Beam X-Ray Luminescence Computed Tomography," *Journal of Modern Optics* 65 (2018): 2278–2289.

45. Z. Zhang, Y. Xu, J. Yang, X. Li, and D. Zhang, "A Survey of Sparse Representation: Algorithms and Applications," *IEEE Access* 3 (2015): 490–530.

46. G. Grossi, R. Lanzarotti, and J. Lin, "Orthogonal Procrustes Analysis for Dictionary Learning in Sparse Linear Representation," *PLoS One* 12 (2017): e0169663.

47. B. Parvitte, C. Risser, R. Vallon, and V. Zéninari, "Quantitative Simulation of Photoacoustic Signals Using Finite Element Modelling Software," *Applied Physics B* 111 (2013): 383–389.

48. N. Ren, J. Liang, X. Qu, J. Li, B. Lu, and J. Tian, "GPU-Based Monte Carlo Simulation for Light Propagation in Complex Heterogeneous Tissues," *Optics Express* 18 (2010): 6811–6823.

49. G. Zhang, J. Zhang, Y. Chen, et al., "Logarithmic Total Variation Regularization via Preconditioned Conjugate Gradient Method for Sparse Reconstruction of Bioluminescence Tomography," *Computer Methods and Programs in Biomedicine* 243 (2024): 107863.